Supporting Information

Ferroelasticity and Canted Antiferromagnetism in Two-Dimensional Organic-Inorganic Layered Perovskite $[C_6H_9(CH_2)_2NH_3]_2FeCl_4$

Naoto Tsuchiya,[†] Tatsuya Ishinuki,[†] Yuki Nakayama,[†] Xianda Deng,[£] Goulven Cosquer,[‡,§]

Takahiro Onimaru,[£] Sadafumi Nishihara[†,‡,¶] and Katsuya Inoue[,†,‡,§]*

†Chemistry Program, Graduate School of Advanced Science and Engineering, Hiroshima University, 1-3-1 Kagamiyama, Higashi-Hiroshima, Hiroshima 739-8526, Japan

‡Chirality Research Center (CResCent), Hiroshima University, 1-3-1 Kagamiyama, Higashi-Hiroshima, Hiroshima 739-8526, Japan

§International Institute for Sustainability with Knotted Chiral Meta Matter (WPI-SKCM^2), Hiroshima University, 1-3-1 Kagamiyama, Higashi-Hiroshima, Hiroshima 739-8526, Japan

£Quantum Matter Program, Graduate School of Advanced Science and Engineering, Hiroshima University, 1-3-1 Kagamiyama, Higashi-Hiroshima, Hiroshima 739-8530, Japan

¶Precursory Research for Embryonic Science and Technology (PREST), Japan Science and Technology Agency (JST), 4-1-8, Honcho, Kawaguchi, Saitama 332-0012, Japan

*e-mail: kxi@hiroshima-u.ac.jp

Table S1. Crystallographic parameters for CHEA-Fe at 173 (*FA*-2), 273 (*FA*-1) and 373 K (*PA*).

Formula		$C_{16}H_{32}N_2FeCl_4$	
Formula weight		450.09	
Temperature / K	173	273	373
Phase	*FA*-2	*FA*-1	*PA*
Crystal system	Monoclinic	Orthorhombic	Tetragonal
Space group (no.)	$P2_1/c$ (14)	*Pnma* (62)	$I4/mmm$ (139)
a [Å]	20.169(2)	20.7316(4)	5.2435(2)
b [Å]	10.2342(11)	39.8114(7)	5.2435(2)
c [Å]	10.2511(11)	5.20440(10)	39.864(3)
β [°]	98.715(4)	90	90
Volume [Å^3]	2091.5(4)	4295.47(14)	1096.02(12)
Z	4	8	2
Density (cal.) [g cm^{-3}]	1.429	1.392	1.364
Absorption coefficient [mm^{-1}]	1.233	1.200	1.176
F(000)	944	1888	472
Reflections collected	11654	30128	4376
Independent reflections	3850	3845	354
Goodness-of-fit on F^2	1.086	1.059	1.279
R_1 [$I > 2\sigma(I)$]	0.1121	0.0678	0.0468
wR_2 [all data]	0.3037	0.1943	0.1343
Largest diff. peak/hole [e Å^{-3}]	2.97/−1.25	0.60/−0.32	0.49/−0.64

Table S2. Selected bond lengths (Å) and bond angles (˚) for CHEA-Fe at 373, 273 and 173 K.

373 K (*PA*)			
Fe(1)–Cl(1)	2.62175(11)	Fe(1)–Cl(2)	2.342(3)
Fe(1)–Cl(1)–Fe(1)^{i}	180		
Symmetry codes: ^{i}+x, +y+1, +z			
273 K (*FA*-1)			
Fe(1)–Cl(1)	2.552(3)	Fe(1)–Cl(2)	2.588(3)
Fe(1)–Cl(3)^{ii}	2.596(3)	Fe(1)–Cl(5)	2.3591(16)
Fe(2)–Cl(2)	2.585(3)	Fe(2)–Cl(3)	2.600(3)
Fe(2)–Cl(4)	2.6516(19)	Fe(2)–Cl(6)	2.3550(16)
Fe(1)–Cl(1)–Fe(1)^{iii}	179.60(11)	Fe(1)–Cl(2)–Fe(2)	178.47(8)
Fe(2)–Cl(3)–Fe(1)^{iv}	179.91(10)	Fe(2)–Cl(4)–Fe(2)^{iii}	179.57(10)
Symmetry codes: ^{ii}+x+1/2, +y, -z-1/2; ^{iii}+x, +y, +z+1; ^{iv}+x-1/2, +y, -z-1/2			
173 K (*FA*-2)			
Fe(1)–Cl(1)	2.556(3)	Fe(1)–Cl(2)	2.555(3)
Fe(1)–Cl(3)	2.384(3)	Fe(1)–Cl(4)	2.370(3)
Fe(1)–Cl(1)–Fe(1)^{v}	165.59(9)	Fe(1)–Cl(2)–Fe(1)^{vi}	179.35(10)
Symmetry codes: ^{v}-x+1, +y+1/2, -z+3/2; ^{vi}+x, -y+1/2, +z+1/2			

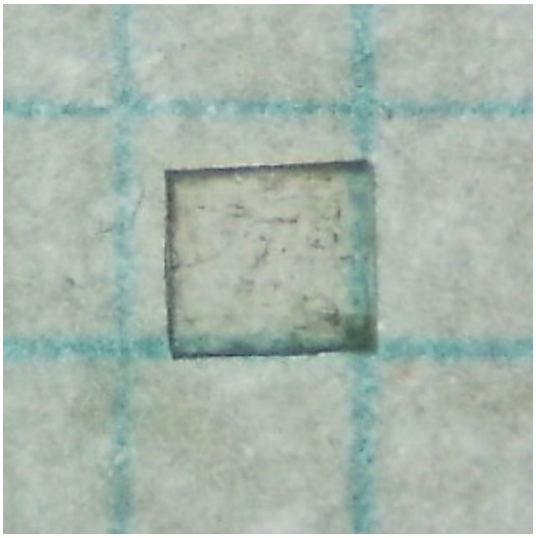

Figure S1. Photo of CHEA-Fe single crystal on millimeter graph paper.

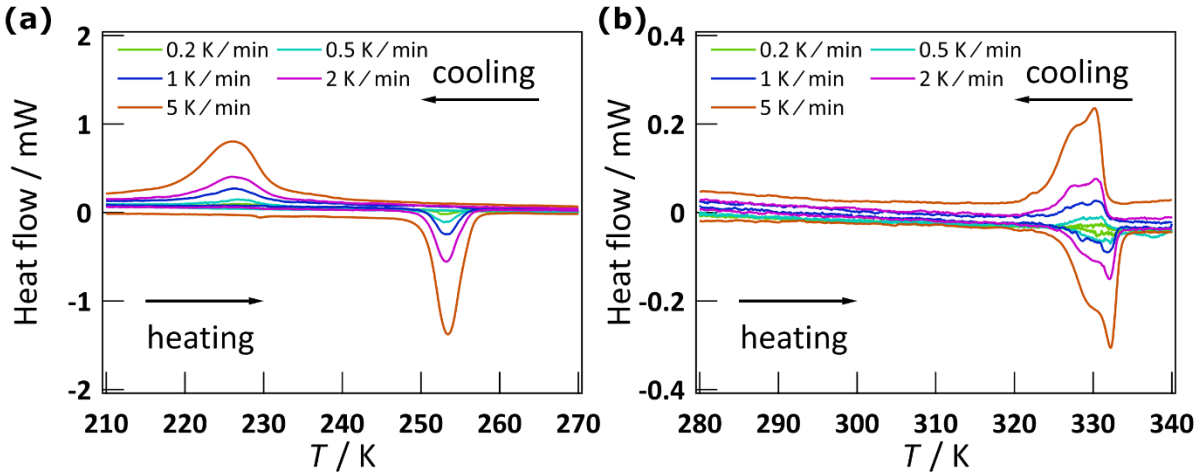

Figure S2. Differential scanning calorimetry data of CHEA-Fe in the temperature range of (a) 210–270 K and (b) 280–340 K with a heating/cooling rate of 0.2, 0.5, 1, 2 and 5 K min^{-1}.

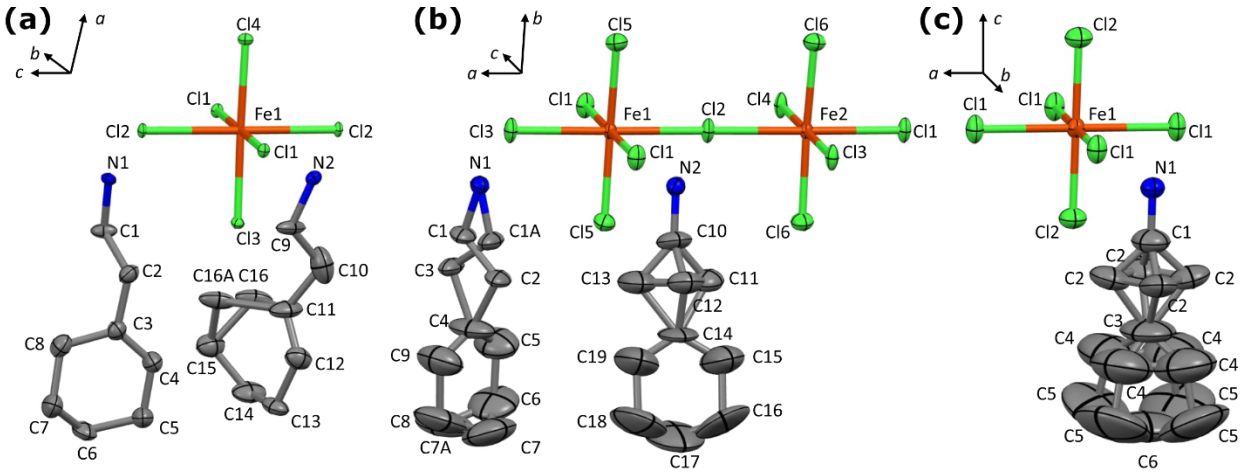

Figure S3. Views of $FeCl_6$ octahedrons and CHEA for CHEA-Fe at (a) 173 K, (b) 273 K and (c) 373 K. Hydrogen atoms are omitted for clarity. Drawings of all atoms are made with thermal ellipsoids of 30% probability. Color codes: Fe, orange; Cl, green; N, blue; C, gray.

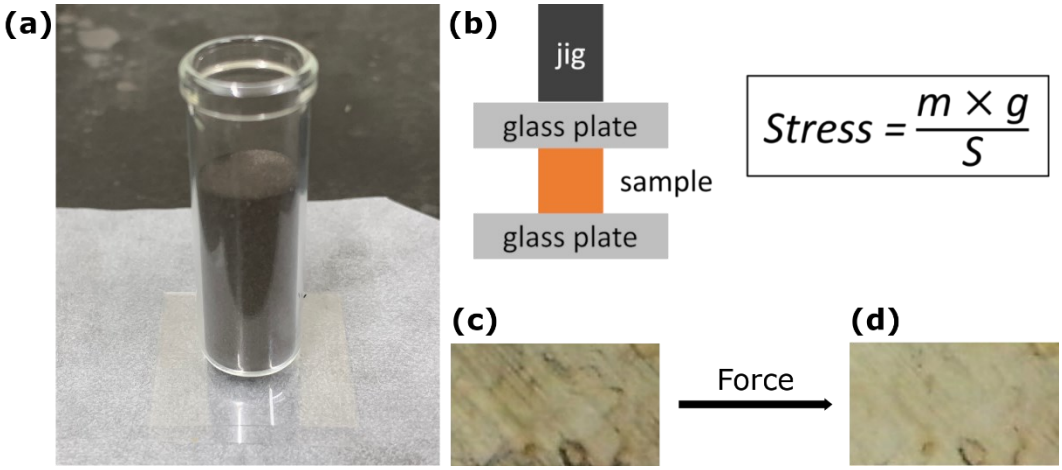

Figure S4. (a) The homemade set-up for applying pressure. A crystal was adhered with araldite glue to glass plates and pressed using a vial loaded with metallic powder (jig). (b) The schematic figure of the homemade set-up, and calculation method of a stress to sample. *m* is the weight of the jig and top glass plate; *g* is the gravitational acceleration and *S* is the cross-sectional area on the interface between the crystal and the top plate. (c,d) Photographs of the multi-domain crystal before applying stress and the single-domain crystal after applying stress at 300 K, respectively.

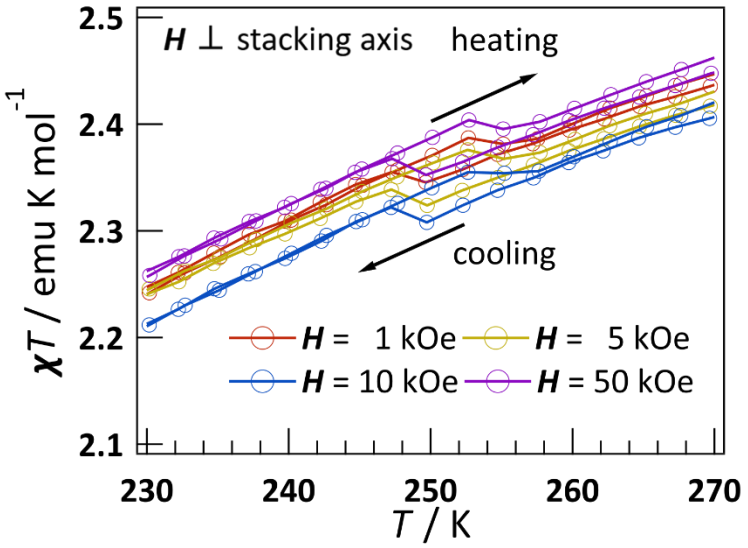

Figure S5. Temperature dependences of χT in the range of 230–270 K for CHEA-Fe when the magnetic field of 1, 5, 10 and 50 kOe is applied perpendicular to the stacking axis.

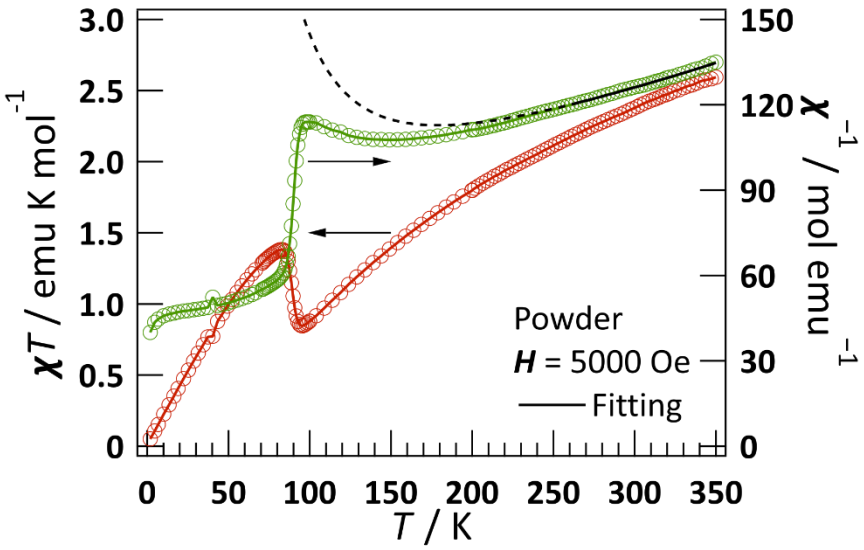

Figure S6. Temperature dependence of χT and χ^{-1} in the range of 2–350 K for powder of CHEA-Fe. The black solid and dash lines show the fit of the experimental result for the model of Heisenberg quadratic-layer antiferromagnet, and its extrapolated curve, respectively (see main text).

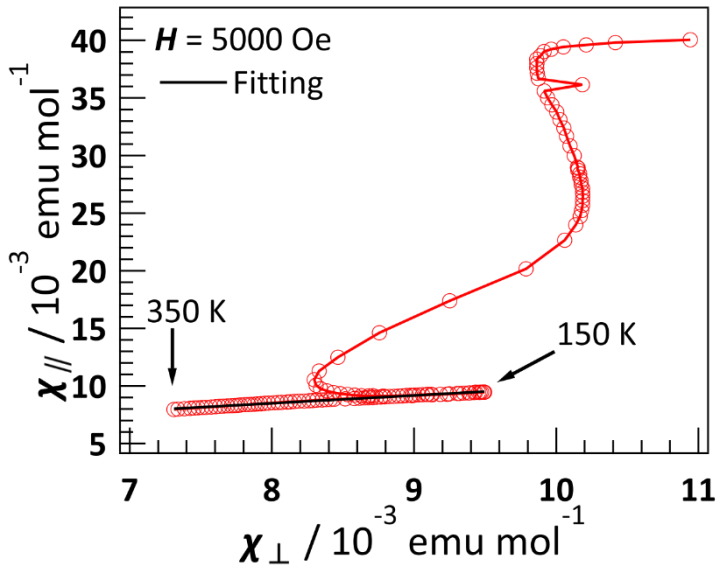

Figure S7. $\chi_{\parallel}$ vs $\chi_{\perp}$ for CHEA-Fe. The black line represents the best fit for applying the linear regression between 350 K and 150 K. The slope of the linear regression corresponds to $(g_{//}/g_{\perp})^2$ as described in the main text.

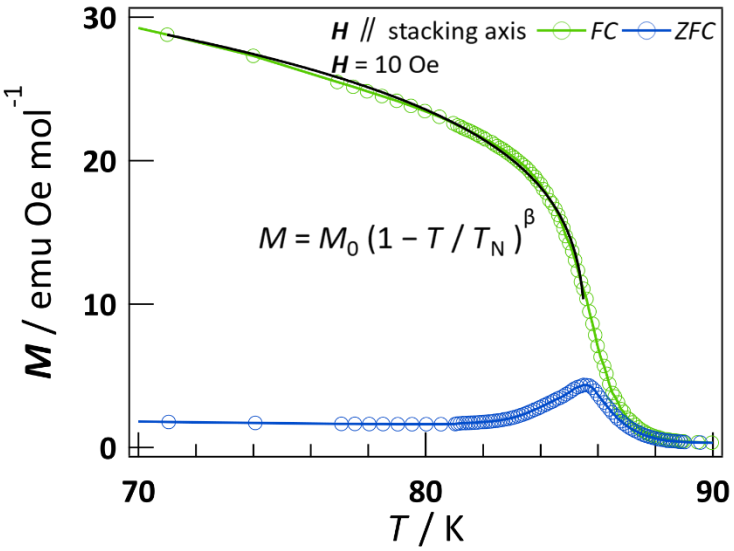

Figure S8. The magnetization vs temperature plots after zero-field cooling (ZFC) and field cooling (FC) of a single crystal in an applied field of 10 Oe along the stacking axis in the region of 70–90 K. The black line represents the best fit of the experimental result for the power law defined as $M = M_0(1 - T/T_N)^{\beta}$.

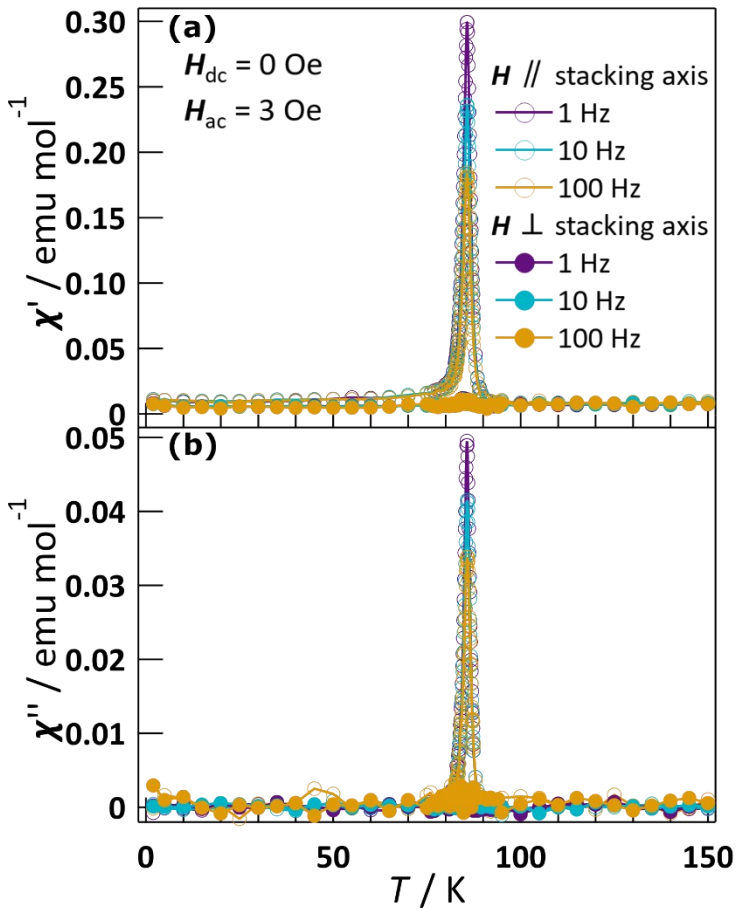

Figure S9. Temperature dependence of (a) the in-phase and (b) the out-of-phase of the AC susceptibilities under zero dc magnetic field for CHEA-Fe when the AC magnetic field of 3 Oe with 1,10 and 100 Hz is applied parallel and perpendicular to the stacking axis.

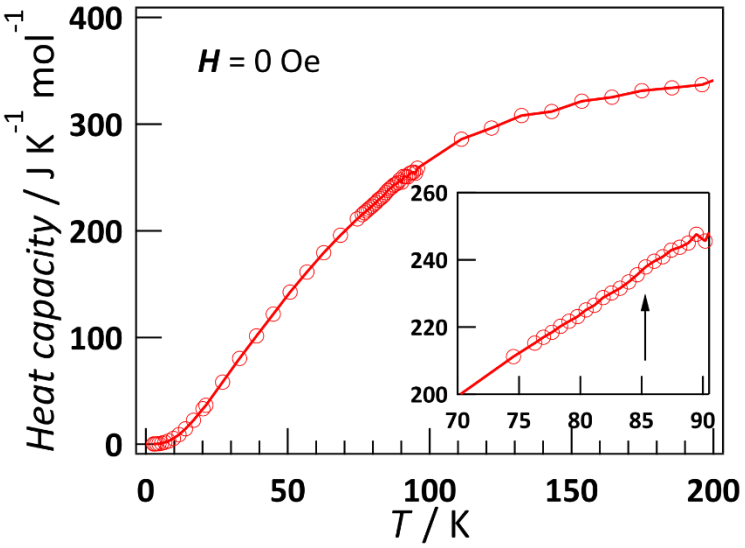

Figure S10. Temperature dependence of the heat capacity for CHEA-Fe. Inset: The temperature dependence of heat capacity in the range of 70–90 K. The arrow presents the temperature of magnetic long-range order.

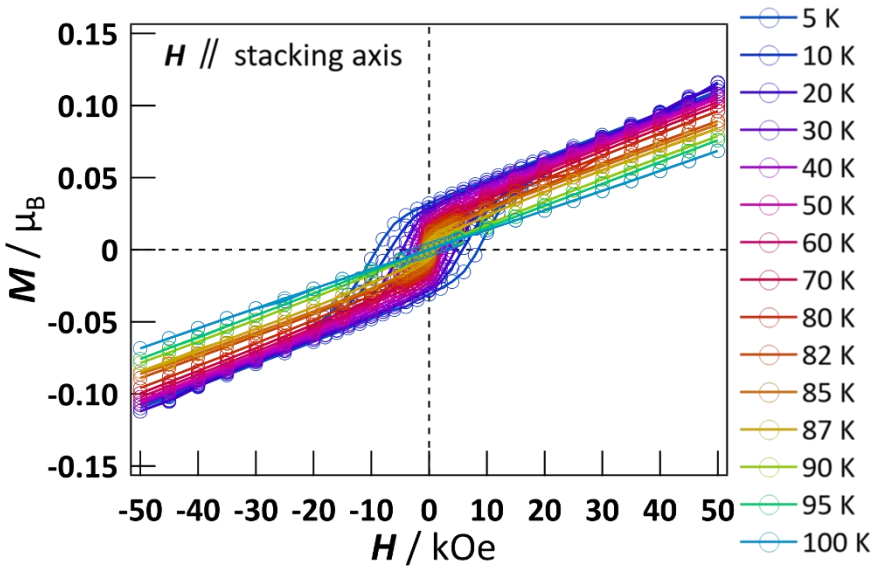

Figure S11. Field dependences of magnetization along the stacking axis at various temperatures for CHEA-Fe.

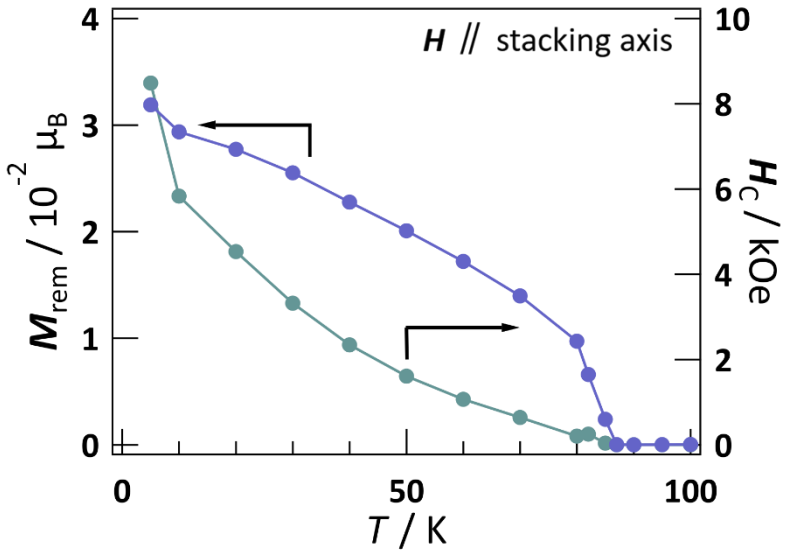

Figure S12. The plots of remanent magnetization (M_{rem}) and coercive field (H_C) derived from the field-dependent magnetization data for CHEA-Fe under 5–100 K with an applied magnetic field along the stacking axis.